ISBN: 978-3-95450-240-0 ISSN: 2673-5547 doi:10.18429/JACoW-HIAT2022-TH2C4

SIGNAL ESTIMATION AND ANALYSING OF COLD BUTTON BPMs FOR A LOW-BETA HELIUM / PROTON SUPERCONDUCTING LINAC*

Y. Zhang†, X. J. Hu, Z. X. Li, H. Jia, S. H. Liu, H. M. Xie
Institute of Modern Physics, Chinese Academy of Sciences, Lanzhou, China

Abstract

We develop a formula including the low-beta effect and the influence of long cable issues for estimating the original signal of cold BPMs. A good agreement between the numerical and the measured signal with regard to two kinds of beam commissioning, helium and proton beams, in a low-beta helium and proton superconducting linac, proves that the developed numerical model could accurately estimate the output signal of cold button BPMs. Analysing the original signal between the first and the last cold BPM in the cryomodule, it is found that the signal voltage in the time domain is increased with the accelerated beam energy. However, the amplitude spectra in the frequency domain has more high frequency Fourier components and the amplitude at the first harmonic frequency reduces a lot. It results in a decline of the summed value from the BPM electronics. The decline is not proportional to a variety of the beam intensity. This is the reason why BPMs give only relative intensity and not absolute value for low-beta beams with a Gaussian distribution.

INTRODUCTION

Cold button BPM, as a normal diagnostic element in the Cryomodules (CMs), play an important function for monitoring the beam position, phase, and energy. Using the summed values from cold button BPMs to measure the beam intensity is our desirable thing. Thus, for a low-beta ion beam, estimating the original signal of cold button BPMs is important since the induced imaging bunch shape is expanded. Furthermore, the signal will be transmitted through a long cable to the electronics. An influence of cable's attenuation and dispersion on the transmission should be confirmed. If an accurate signal estimation in the time domain (TD) could be proven, we could perform the Fast Fourier Transform (FFT) to obtain the amplitude spectra in the frequency domain (FD) and analyse what signal is processed in the digital electronics. At last, we find the summed values of cold button BPMs processed by the digital electronics are decreasing along the superconducting (SC) linac. We will discuss these unexpected summed values and prove that they could not be used for monitoring the absolute beam intensity in a low-beta SC Linac

CAFe AND ITS COLD BUTTON BPMs

CAFe is a low-beta helium / proton superconducting LINAC. It is as a demo LINAC for China initiative Accelerator-Driven System and constructed at the Institute of Modern Physics, Chinese Academy of Science, as shown in Fig. 1. This facility includes two ion sources with an output energy of 20 keV/u before a 4-vane type copper structure radio frequency quadrupole (RFQ) with an accelerated energy of 1.5 MeV/u. The first is an electron cyclotron resonance (ECR) proton source of 10 mA with an energy of 20 keV, and the second includes an ECR helium source of 2 mA. After the RFQ section, they have the same layout, including a medium energy beam transport (MEBT), four cryomodules (CMs) and a high energy beam transport (HEBT) line. In four CMs, there are 23 half-wave resonance (HWR) SC cavities, 23 SC solenoids, and 19 cold button BPMs [1-3].

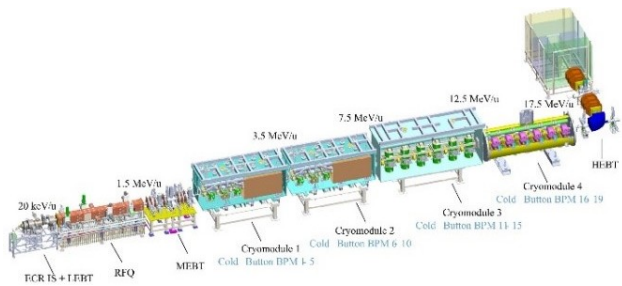

Figure 1: Schematic layout of Chinese ADS Front-end superconducting demo LINAC (CAFe).

Cold Button BPMs are both nonlinear and dependent on the position in the orthogonal plane. A general rule of thumb is that the button width should be approximately 60° wide, leaving a 30° gap between buttons. An initial design and test of the system was published in Ref. [4]. Our button parameter is optimized to an angular coverage ϕ of 62.2° to obtain high sensitivity. The surface is shaped as a section of a cylinder to be flush with the vacuum chamber surface, as shown in Fig. 2.

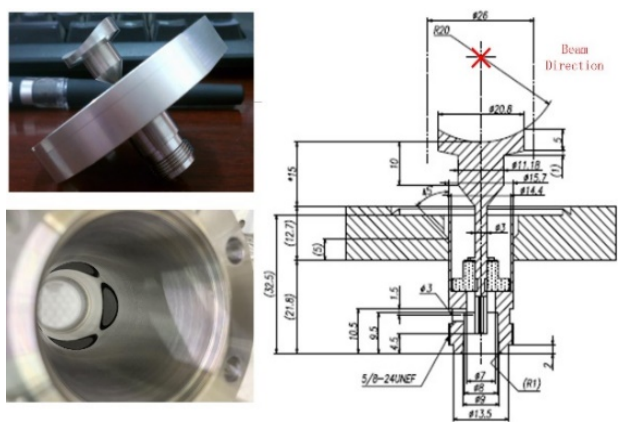

Figure 2: Button electrode, assembling picture and its drawing [4].

* Work was supported by National Natural Science Foundation of China (Grant No. 11675237) and the 2018 "Western Light" Talents Training Program of Chinese Academy of Sciences.
† zhangy@impcas.ac.cn

ISBN: 978-3-95450-240-0 ISSN: 2673-5547 doi:10.18429/JACoW-HIAT2022-TH2C4

DESCRIPTION OF TWO KINDS OF BEAM COMMISSIONING

From the middle of 2020 to the beginning of 2021, there were two kinds of beam commissioning. One was Helium-4 ion beams with a peak current of 145 μA at an energy of 6–7 MeV/u, and the other was proton beams with a peak current of 4–10 mA at an energy of 16–20 MeV [3]. There are two ACCTs (AC current transformer from Bergoz Instruments, ACCT-CF6"-60.4-40 UHV) in the entrance of CM1 and the exit of CM4, respectively, to monitor the peak current [5]. Beam current is obtained by a data acquisition card with the sampling rate of 20 MHz/s (made in-house). It is recorded in a data base. The original data from cold button BPM 1 and 19 are obtained by an oscilloscope at the same time for the analysis. We choose the recorded current data during the obtaining time and show them in Fig. 3 and Fig. 4. The related beam size and energy at the location of cold button BPM1 and 19 are listed in Table 1. The beam orbit has been tuned to the center within less than 2 mm to prevent beam losses. In the next part, the signal estimation and the comparison of cold button BPMs are all based on the above-mentioned data.

Table 1: Parameters of Beam Size and Energy for Cold BPM1 and BPM19 During Two Kinds of Beam Commissioning

Beam parameters		$^4He^{2+}$		Proton	
		cold BPM1	cold BPM19	cold BPM1	cold BPM19
X_{rms}	[mm]	1.66	1.93	1.51	1.31
Y_{rms}	[mm]	1.66	2.84	1.42	1.31
Z_{rms}	[°]	4.64	3.82	4.3	1.89
Energy	[MeV/u]	1.59	6.89	1.78	16.93

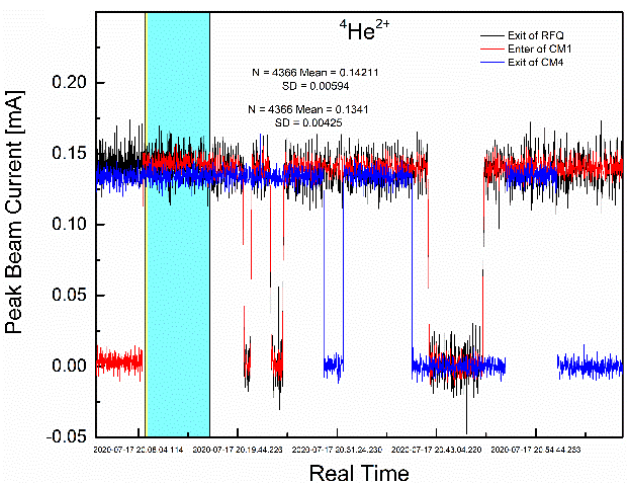

Figure 3: $^4He^{2+}$ beams' current in real time (from 20:08 to 20:54 on July 17, 2020).

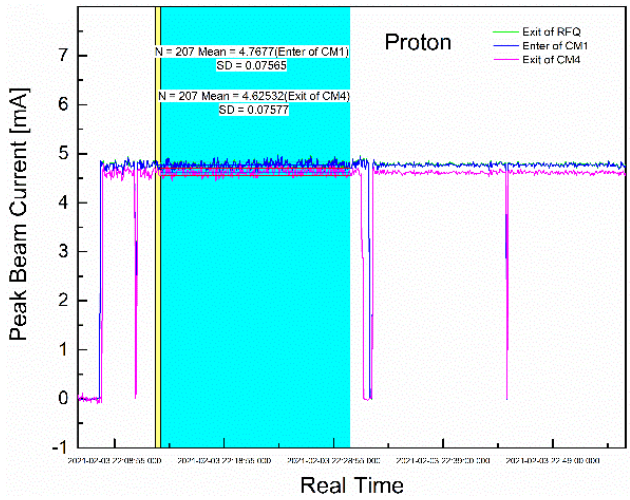

Figure 4: Proton beams' current in real time (from 22:08 to 22:49 on February 3, 2021).

SIGNAL ESTIMATION OF COLD BUTTON BPMs

3D Model and Simulated Results by CST PS

An accurate 3D model of cold button BPM is developed in SOLIDWORKS and then imported to CST PS for the simulation [6, 7]. The button electrode parameters are the same as the described in the last Section. Using an E-field monitor and voltage monitor, the output voltage of the electrode is simulated. A distribution of the bunched beam current and the related output voltage of cold BPM1 for $^4He^{2+}$ beams are simulated by CST PS with a PIC solver, as shown in Fig. 5. Furthermore, a numerical model is developed to check the simulated results.

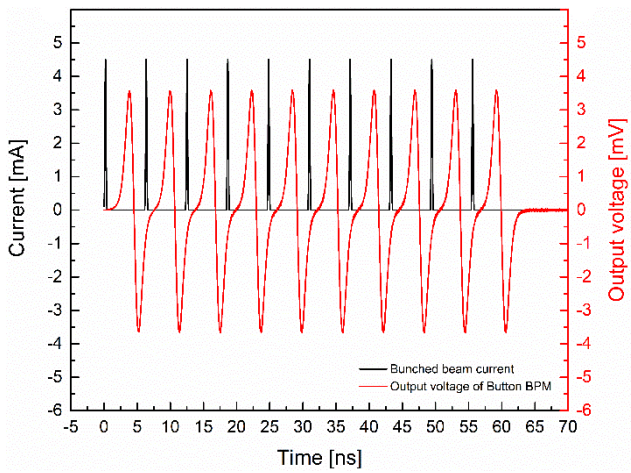

Figure 5: Simulated distribution of the bunched beam current and the output voltage of cold button BPM1 by CST PS with PIC solver.

ISBN: 978-3-95450-240-0 ISSN: 2673-5547 doi:10.18429/JACoW-HIAT2022-TH2C4

Numerical Model and Comparisons of the Output Signal from Cold Button BPMs

Considering a Gaussian bunch shape, the beam current $I_b(t)$ of a single bunch is given by [8]:

$$I_b(t) = \frac{eN}{\sqrt{2\pi}\sigma} \cdot e^{\left(\frac{-t^2}{2\sigma^2}\right)}, \quad (1)$$

where N is the total particle number and σ is the rms bunch length. Assuming a symmetric bunch shape in time with a bunching period of T, the repetitive beam current could be represented by Fourier series expansion in TD as:

$$I_b(t) = \langle I_b \rangle + 2\langle I_b \rangle \cdot \sum_{m=1}^{\infty} A_m \cdot \cos(m\omega_0 t), \quad (2)$$

where $\langle I_b \rangle$ is the average dc current, ω_0 is the bunching angular frequency, m is the harmonic, and

$$A_m = e^{\left(\frac{-m^2\omega_0^2\sigma^2}{2}\right)}.$$

The length of the image charge distribution (opposite sign) is wider than the physical length of the bunch charge distribution for the low-β beam. The length of the image charge of the bunch is assumed,

$$\sigma_{im}^2 = \sqrt{\sigma^2 + \left(\frac{b}{\sqrt{2}\beta\gamma c}\right)^2},$$

where σ is the rms longitudinal bunch length, b is the radius of the beam pipe, βc is the beam velocity, and γ is the relativity factor.

Thus, the image current can be rewritten as:

$$I_{im}(t) = -\langle I_b \rangle - 2\langle I_b \rangle \cdot \sum_{m=1}^{\infty} B_m \cdot \cos(m\omega_0 t), \quad (3)$$

where

$$B_m = e^{\left(\frac{-m^2\omega_0^2\sigma_{im}^2}{2}\right)}. \quad (4)$$

The button electrode voltage on a termination of R is

$$V_{\text{button}}(t) = R \cdot i_s(t) = \frac{\Phi l R}{2\pi\beta c} \cdot \frac{dI_{im}(t)}{dt}. \quad (5)$$

Substituting Eqs. (3) and (4) into Eq. (5), the voltage of the button electrode for the low-β bunched ion beam is:

$$V_{\text{button}}(t) = -\langle I_b \rangle \cdot \frac{\Phi l R}{2\pi\beta c} \cdot \cdot \sum_{m=1}^{\infty} e^{\left(\frac{-m^2\omega_0^2\sigma_{im}^2}{2}\right)} \cdot (-m\omega_0) \cdot \sin(m\omega_0 t), \quad (6)$$

where the factor ϕl is equal to the button electrode surface area divided by b. Using Eqs. (2), (3) and (6), the bunched current distribution of low-β beams, its image current distribution and the related output signal of the button electrode are numerically calculated by a MATLAB code [9] and plotted in Fig. 6. There is a comparison between the CST simulated, the numerical calculated by Eq. (6) and the measured original signal from cold BPM1, shown in Fig. 7. It indicates that the assumed imaging bunch length for low-β

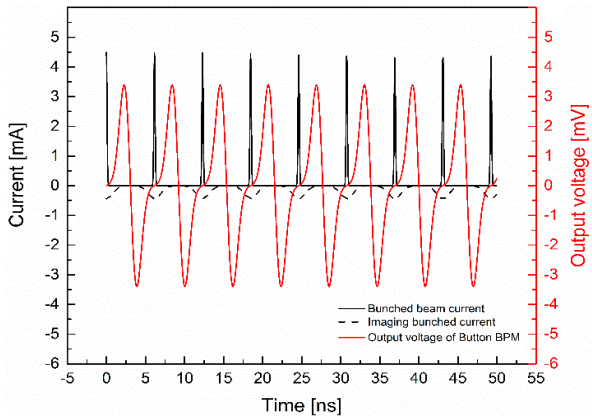

Figure 6: Numerical calculated distribution of the bunched beam current, image current and related output voltage of the button electrode by Eq. (2), Eq. (3) and Eq. (6).

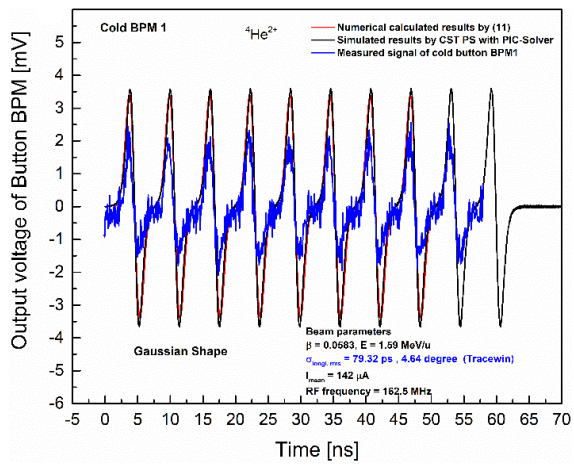

Figure 7: Comparisons between the simulation by CST PS with PIC solver, the numerical calculation by Eq. (6) and the measured output voltage of cold button BPM1.

beams is right. However, there is a large difference in the amplitude between the measured and the simulated values. This is due to the measured signal from the oscilloscope through a long cable transmission connected to the button electrode. The long cable transmission leads to an asymmetric measured signal. Thus, CST simulation and formula (6) only consider the output signal directly from the electrode. Furthermore, the signal estimation of cold button BPM including the influence of cable attenuation and dispersion is presented as the following.

If the bipolar output signal of the cold button pick-up can be written in the model (6), the signal with cable attenuation and dispersion could perform a convolution operation on Eq. (6). Then the complete expression for the attenuated button pick-up signal including cable attenuation and dispersion is Eq. (7), where αm is the attenuation per unit length at frequency with the unit of nepers per meter. τ is the frequency-independent insertion delay for a lossless cable of length z. Other factors keep the same definition as listed in Eq. (6). The amplitudes of the individual frequency components are attenuated following the $f^{1/2}$ rule, and their relative phases are skewed because of the frequency-dependent dis-

ISBN: 978-3-95450-240-0 ISSN: 2673-5547 doi:10.18429/JACoW-HIAT2022-TH2C4

persion in the transmission line. In our case, the measured raw signal of cold button BPMs is obtained from an Agilent 90604A oscilloscope port, which is connected to a transmission line including a cold button feedthrough (port A), a 2.3 meter semirigid RF cable in CM, and a 30 m RF cable (TCOM240-PUR-FR from Times Microwave Systems) in the air.

$$V_{\text{button}}(t) = -\langle I_b \rangle \cdot \frac{\Phi l R}{2\pi\beta c} \cdot \sum_{m=1}^{\infty} \left\{ e^{\left(-\alpha_m \sqrt{f} z\right)} \cdot e^{\left(\frac{-m^2\omega_0^2\sigma_{im}^2}{2}\right)} \cdot (-m\omega_0) \cdot \sin\left(m\omega_0(t-\tau) - \alpha_m\sqrt{f}z\right) \right\} \quad (7)$$

Here, we only consider the influence of 30-meter cables since the specifications of semirigid RF cables are not very clear. We assume the semirigid cable with the same specification as TCOM240. Then, the total length z of cables is approximately 33 m, with respect to the time delay τ of 131 ns (= 33/0.84/(3×108)).

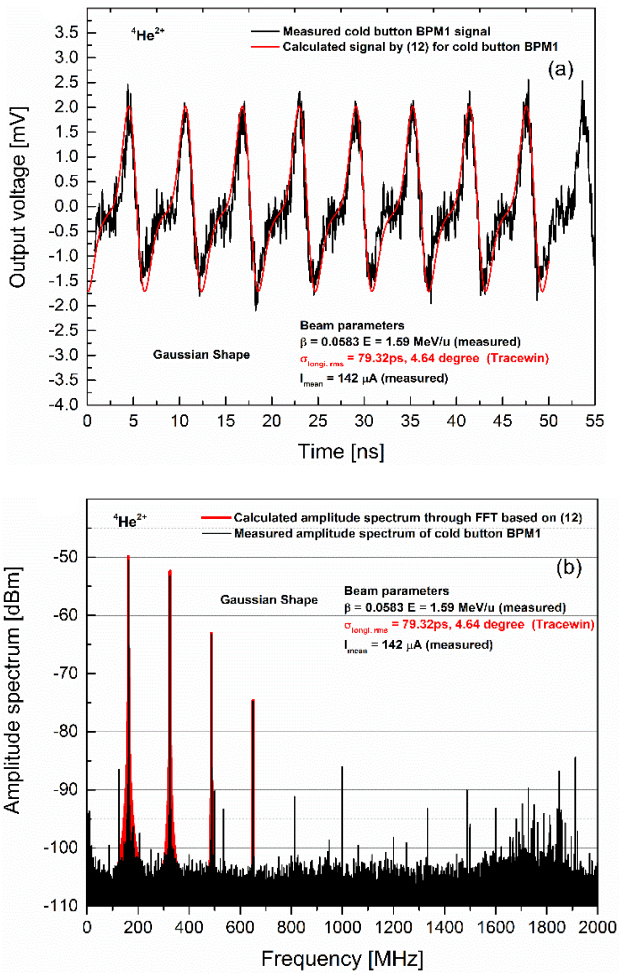

Figure 8: Comparisons between the calculated by Eq. (7) and the measured output voltage of cold button BPM1 in TD (a) and FD (b) during $^4He^{2+}$ beam commissioning.

The TCOM240 cable attenuation is calculated in neper per meter by [10] $\alpha_m = (0.229148 \cdot \sqrt{F\text{MHz}} + 0.000331 \cdot F\text{MHz})/33/8.6$.

Substituting τ, z and α_m into Eq. (7), the numerical signal of the cold button BPM considering the low-β effect, cable attenuation and dispersion can be obtained.The measured and the calculated results for $^4He^{2+}$ beams and proton beams are compared and presented in Figs. 8 and 9. When a centred $^4He^{2+}$ beam with current of 142 μA enters the first SRF cavity, port A of cold button BPM1 shows an original signal with an asymmetric peak-to-peak voltage Vpp of 2 mV. The calculated result by Eq. (7) shows a good agreement with the measured in terms of the amplitude and shape, as shown in Fig. 8(a). The amplitude spectra in FD are transformed based on the estimated signal in TD. The spectra in FD also is coincided with the measured at the main harmonic frequencies (1st, 2nd, 3rd, 4th), as shown in Fig. 8(b). When proton beams with current of 4.76 mA enters the first SRF cavity and exits CM4 with current of 4.62 mA, port A of cold buttons BPM19 shows the original signals with asymmetric Vpp values of 135 mV, as shown in Fig. 9(a). Correspondingly, the amplitude spectra in FD is coincided with together, as shown in Fig. 9(b). The induced imaging bunch shape and the amplitude of signal could have a good agreement with the measured results regardless of whether the signal is

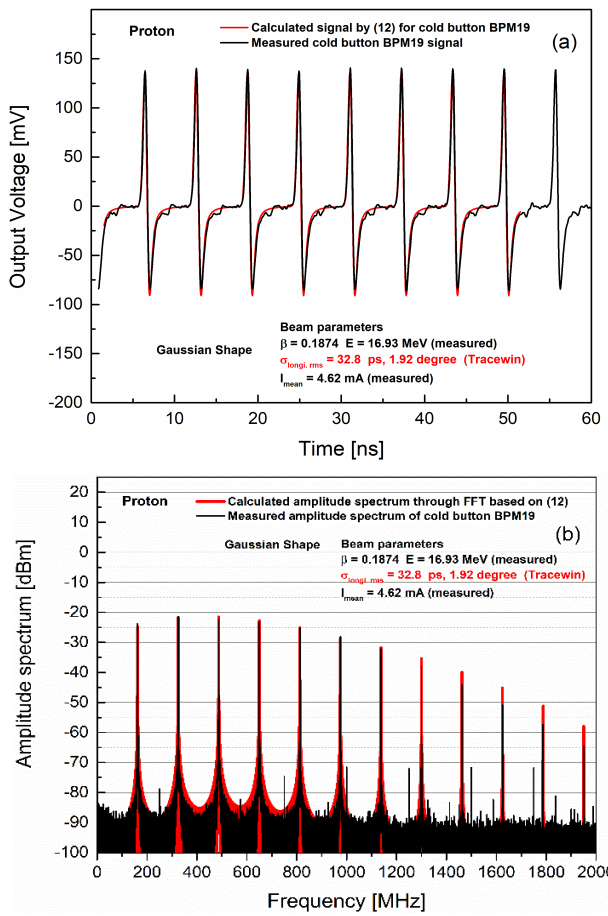

Figure 9: Comparisons between the calculated by Eq. (7) and the measured output voltage of cold button BPM19 in TD (a) and FD (b) during proton beam commissioning.

ISBN: 978-3-95450-240-0 ISSN: 2673-5547 doi:10.18429/JACoW-HIAT2022-TH2C4

from the helium beam or from the proton beam with different energies. At the same time, there is in agreement with the amplitude spectra in FD.

ANALYSIS OF SUMMED VALUES FOR COLD BUTTON BPMs

Based on the above results, we could use numerical model Eq. (7) to analyse the summed signal of cold button BPM1 and BPM19 with the centred beam. As shown in Figs. 3 and 4, the transmission efficiency from the entrance to the exit of CMs is approximately 95% (= (142 – 134) / 142) and 97.1% (= (4.76 - 4.62) / 4.76) during two kinds of beam commissioning, a low-power $^4He^{2+}$ beam and a high-power proton beam. As shown in Fig. 10, four color curves present Va, Vb, Vc, and Vd signals of cold button BPMs from the Libera Single Pass H (LSPH) [11]. For each BPM, four

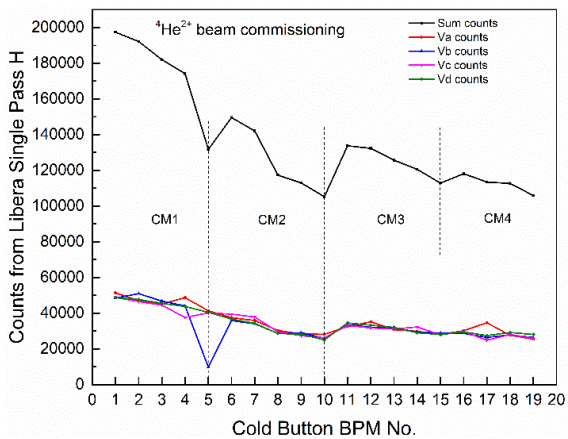

Figure 10: Trends of Sum, Va, Vb, Vc and Vd from cold button BPM1 to BPM19. These data are from the BPM electronics of Libera Single Pass H. The recording time is from 20:50 to 20:54 on July 17, 2020.

values remain similar except cold BPM5 since its Vb is very small. This means that $^4He^{2+}$ beam is around the center position. The summed values of four port signals (= Va+Vb+Vc+Vd) continue to decline in the counts, as shown in the black curve. The decrease ratio of summed values between BPM19 and BPM1 is up to 46% (= (1.97×10^5 - 1.06×10^5) / 1.97×10^5). However, the beam current just has losses of 5%. Similarly, we perform the same comparison for proton beam. As shown in Fig. 11, the summed values between cold buttons BPM1 and BPM19 from LSPH has decreased by 44% (= (8.9×10^5 – 4.96×10^5) / 8.9×10^5). However, the beam current difference is only 2.9%.

For our BPM electronics, LSPH uses narrowband processing to obtain a higher precision of the position reading. The summed counts of LSPH shown in Figs. 10 and 11 are all acquired at the first frequency. In fact, during a routine beam commissioning, it is not permitted to obtain the original signal of cold button BPMs through oscilloscopes because of the requirement from machine protect system (MPS). Thus, the numerical model Eq. (7) plays an important role to help us understand the raw signals of cold button

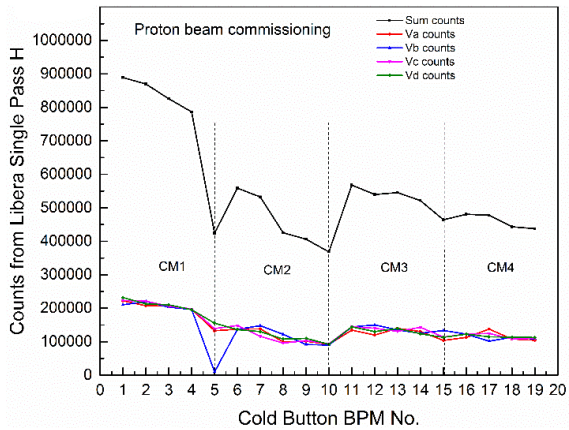

Figure 11: Trends of Sum, Va, Vb, Vc and Vd from cold button BPM1 to BPM19. These data are from the BPM electronics of Libera Single Pass H. The recording time is from 22:08 to 22:49 on Feb. 3, 2021.

BPMs, as shown in Figs. 12 and 13. Through FFT transforming from TD to FD on the calculated signal, it is found that the calculated differences between BPM1 and BPM19 are

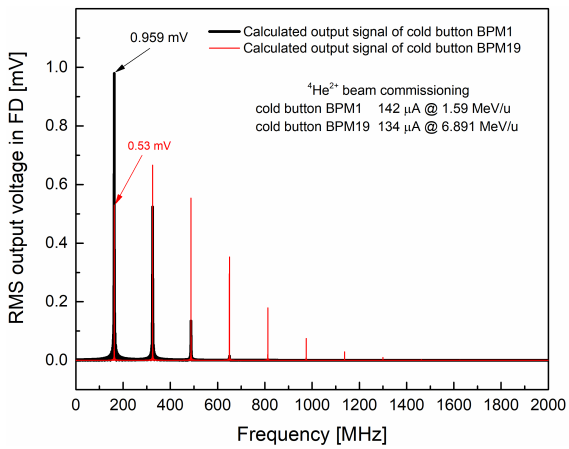

Figure 12: Comparison between the calculated signal in FD of cold button BPM1 and BPM19 during $^4He^{2+}$ beam commissioning.

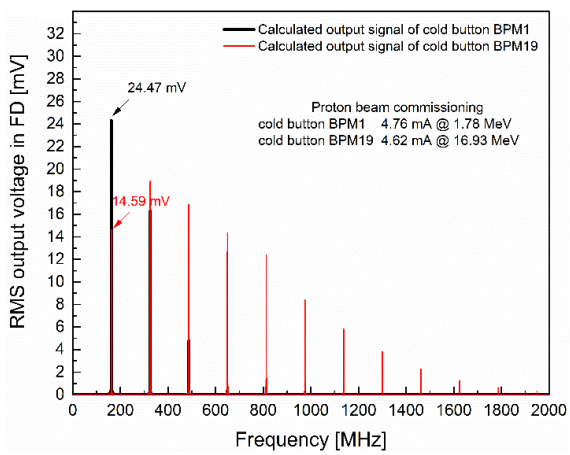

Figure 13: Comparison between the calculated output signal in FD of cold button BPM1 and BPM19 during proton beam commissioning.

ISBN: 978-3-95450-240-0 ISSN: 2673-5547 doi:10.18429/JACoW-HIAT2022-TH2C4

44.7% (= (0.959-0.53) /0.959), and 40% (= (24.47-14.59) / 24.47), which are similar to the measured differences at the first harmonic frequency.

For two kinds of beam commissioning, there are some similar conditions. Cold BPM5, the summed counts are particularly small because its Vb is small, as shown in Figs. 10 and 11, which indicates that port B of BPM5 has some problems. In CM2, cold BPM numbers is from 6 to 10. The measured data is smaller than the others. The only difference between CM2 and the others is that the semirigid RF cables are different. In CM2, we use semirigid cables with the dielectric material SiO_2 from MEGGITT. The others use semirigid RF cables with the dielectric material microporus PTFE from Times Microwave Systems. The different insert losses of semirigid cables might result in the summed value difference from cold button BPM6 to BPM10 in CM2. However, it could not change the decreasing trend of summed counts along CMs.

Figures 11 and 13 prove that the amplitude spectra of button BPMs in FD are widened with the beam energy increasing and the longitudinal length shortening, regardless of whether the signal from $^4He^{2+}$ beam or from proton beam. At the same time, the amplitude at the first harmonic frequency of 162.5 MHz is decreasing along the LINAC. Depending on the analysis of original signals in FD from the estimated signals by Eq. (7), we realize that the differential summed values of cold button BPMs could not monitor whether beam current has been lost or not in CMs. The summed values of BPM could only give us the relative current to prove there is a beam in CMs. This changes our interlock strategy for the low-β high-power proton SC LINAC.

CONCLUSION

In this paper, we use the simulated method and the numerical calculation to derive the output signal of button BPMs for a multi-bunched low-β beam. The simulated results from CST PS with the PIC solver and the numerical calculated results based on formula Eq. (6) confirm that the output signal shape width coincides with the measured value, which indicates that the assumed imaging bunch length for low-β beams is correct. Furthermore, we develop model Eq. (7) to estimate the output signal of cold button BPMs. A series of comparisons between the calculated and the measured signals from $^4He^{2+}$ and proton beam commissioning proves model Eq. (7) to be accurate. It could help us understand what signal is processed by BPMs' electronics. Based on the FFT results, the amplitude spectra are expanded and have more high frequency components when the energy increasing and the longitudinal bunch length shortening. At the same time, the amplitude at the basic harmonic frequency of 162.5 MHz decreases, which leads to the summed values from LSPH showing a continuous decline in numbers. Because the BPM electronics LSPH processes the amplitude spectra of BPM signal in FD with a narrowband processing. We realize that the differential values between the different cold button BPMs could not monitor the beam current transmission efficiency. The summed values from cold button BPMs could only give the relative low-β beam intensity. Numerical model Eq. (7) is very useful for designing, estimating, and analysing the button BPM function when facing the centred low-β beam accelerated by an ion/proton low-β SC LINAC.

REFERENCES

[1] Z. Wang, Y. He, H. Jia, *et al.*, "Beam commissioning for a superconducting proton LINAC," *Phys. Rev. Accel. Beams.*, vol. 19, no. 12, pp. 120101, Dec. 2016. doi:10.1103/PhysRevAccelBeams.19.120101

[2] S. H. Liu, Z. J. Wang, H. Jia, Y. He, *et al.*, "Physics design of the CIADS 25 MeV demo facility," *Nucl. Instrum. Methods Phys. Res., Sect. A*, vol. 843, pp. 11-17, 2017. doi:10.1016/j.nima.2016.10.055

[3] *High-power linac shows promise for accelerator-driven reactors*, https://cerncourier.com/a/high-power-linac-shows-promise-for-accelerator-driven-reactors/

[4] Y. Zhang, J. X. Wu, G. Y. Zhu, H. Jia, *et al.*, "Capacitive beam position monitors for the low-β beam of the Chinese ADS proton LINAC," *Chinese Phys. C*, vol. 40, p. 027003, 2016. doi:10.1088/1674-1137/40/2/027003

[5] Bergoz instrumentation, www.bergoz.com

[6] Dassault Systèmes, 3DS, www.3ds.com

[7] Dassault Systèmes, SOLIDWORKS, www.solidworks.com

[8] R. E. Shafer, "Beam position monitoring,'' *AIP Conf. Proc.*, vol. 212, p. 26, 1990. doi:10.1063/1.39710

[9] MathWorks, www.mathworks.com

[10] Times Microwave Systems, www.timesmicrowave.com

[11] I-Tech Instrumentation Technologies, www.i-tech.si